

Rydberg Molecules for Ion-Atom Scattering in the Ultracold Regime

T. Schmid,¹ C. Veit,¹ N. Zuber,¹ R. Löw,¹ T. Pfau,¹ M. Tarana,² and M. Tomza^{3,4}

¹*Physikalisches Institut and Center for Integrated Quantum Science and Technology, Universität Stuttgart, Pfaffenwaldring 57, 70569 Stuttgart, Germany*

²*J. Heyrovský Institute of Physical Chemistry of the ASCR, v.v.i., Dolejškova 2155/3, 18223 Prague 8, Czech Republic*

³*Centre of New Technologies, University of Warsaw, Banacha 2c, 02-097 Warsaw, Poland*

⁴*Faculty of Physics, University of Warsaw, Pasteura 5, 02-093 Warsaw, Poland*

(Dated: March 2, 2022)

We propose a novel experimental method to extend the investigation of ion-atom collisions from the so far studied cold, essentially classical regime to the ultracold, quantum regime. The key aspect of this method is the use of Rydberg molecules to initialize the ultracold ion-atom scattering event. We exemplify the proposed method with the lithium ion-atom system, for which we present simulations of how the initial Rydberg molecule wave function, freed by photoionization, evolves in the presence of the ion-atom scattering potential. We predict bounds for the ion-atom scattering length from *ab initio* calculations of the interaction potential. We demonstrate that, in the predicted bounds, the scattering length can be experimentally determined from the velocity of the scattered wave packet in the case of ${}^6\text{Li}^+ - {}^6\text{Li}$ and from the molecular ion fraction in the case of ${}^7\text{Li}^+ - {}^7\text{Li}$. The proposed method to utilize Rydberg molecules for ultracold ion-atom scattering, here particularized for the lithium ion-atom system, is readily applicable to other ion-atom systems as well.

The considerable achievements made in the field of degenerate quantum gases over the past decades rely on the exact understanding and control of interactions between neutral atoms in the ultracold regime [1, 2]. Considering the interactions between ions and atoms, substantial work has been done in the cold, but essentially classical regime, deploying hybrid ion-atom traps. These hybrid traps combine a Paul trap for the ion with an optical and/or a magnetic trap for the atoms. Both elastic and inelastic collisions have been studied in these traps for various ion-atom combinations [3–5]. However, the ultracold, quantum regime, i.e., the *S*-wave collision regime, could not be reached with any of these systems (see Fig. 1). Cetina, Grier, and Vuletić showed [17] that by the use of a Paul trap there arises a micromotion-induced limit on the minimum collision energy which can be reached. Only for a combination of a heavy ion with a light atom, e.g., the $\text{Ca}^+ - \text{Li}$ or the $\text{Yb}^+ - \text{Li}$ system, might the *S*-wave collision regime be entered. For both of these ion-atom combinations, collision measurements have recently been carried out in the millikelvin energy range [8, 10] which is, however, still in the classical regime. Schaetz and co-workers [18] follow a different path to enter the ultracold regime. To avoid the spurious heating of the ion by the Paul trap, they optically trap the ion, and they are currently working on the simultaneous optical trapping of the ion and the atoms [19].

The generation and characterization of many different types of Rydberg molecules has been an active area of research in the past few years. These molecules consist of a Rydberg atom and at least one ground state atom which is bound to the Rydberg ionic core at a very large internuclear distance via its attractive interaction with the Rydberg electron [20]. Triplet *s*-state Rydberg dimers, trimers, tetramers, and pentamers have

been observed [21–23], and molecular lifetimes have been measured [24, 25]. Furthermore, triplet *d*-state dimers have been studied [26, 27] as well as mixed singlet-triplet dimers [28, 29]. Finally, trilobite [30–33] and butterfly [34] molecules have been investigated.

State-of-the-art *ab initio* calculations could determine the interaction potential of light few-electron systems to such a precision that reliable predictions of the scattering length could be made, e.g., for the scattering of two helium atoms, either in their ground state [35] or in the metastable 2^3S_1 state [36]. Accurate estimations of the scattering length could also be given for weakly interacting many-electron systems with a very small reduced mass, e.g., for metastable helium scattering off alkali-metal atoms [37, 38]. Precisely predicting the scattering length for heavier systems is very challenging, though.

In this Letter, we propose a novel experimental method to extend the investigation of ion-atom interactions from the hitherto studied cold regime to the unexplored ultracold regime. The key aspect of this method is the unprecedented use of a Rydberg molecule as a tool to initialize an ultracold ion-atom scattering event. This makes a separate trap for the ion, be it a Paul trap or an optical trap, expendable. The proposed method allows for the experimental determination of the ion-atom scattering length and thus provides a very valuable benchmark for its *ab initio* calculation.

The starting point of the proposed procedure is the photoassociation of a single Rydberg molecule in an ultracold, dilute atomic cloud. The Rydberg molecule is then photoionized to start the ultracold ion-atom scattering event between the Rydberg ionic core and the ground state atom; i.e., the initial Rydberg molecule wave function, freed by photoionization, evolves in the presence of the ion-atom scattering potential. Depending on the

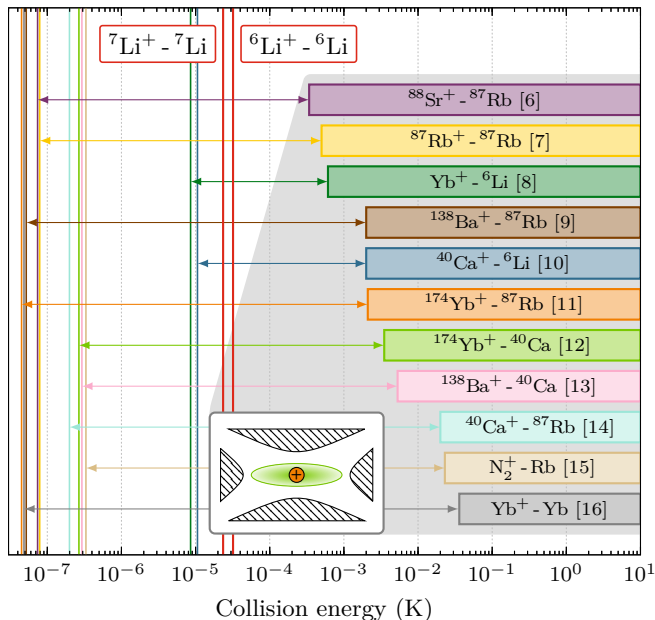


FIG. 1. In the past few years, the ion-atom interaction could be studied down to the millikelvin regime for various ion-atom combinations by the use of hybrid traps, with the ion held in a Paul trap (inset). However, the ultracold, quantum scattering regime could not be reached yet (see color-coded lines for the respective S -wave scattering limits E_0). We propose an experimental method to enter the ultracold ion-atom scattering regime using Rydberg molecules. We demonstrate this method with the lithium ion-atom system which features an early onset of the S -wave scattering regime due to its small reduced mass.

scattering length, either the entire scattered wave packet is free and dispersively expanding, or it splits into a free part and a bound part, indicating the formation of a molecular ion. The detection of the free ion and/or the molecular ion with a time- and position-sensitive single-ion detector concludes the single ultracold ion-atom scattering event. The frequent repetition of this single scattering event eventually allows for the determination of the ion-atom scattering length.

We exemplify the proposed method to enter the ultracold ion-atom scattering regime with the lithium ion-atom system. It features an early onset of the S -wave scattering regime due to its small reduced mass μ . Its S -wave scattering limit $E_0 = (2\mu^2 C_4)^{-1}$ [16] ($C_4 = 164.2$ a.u. [39]) is approximately 2 orders of magnitude larger than the respective limits for the ion-atom systems so far studied in the millikelvin range, except for the $^{40}\text{Ca}^+ - ^6\text{Li}$ and the $\text{Yb}^+ - ^6\text{Li}$ system (see Fig. 1). We present an *ab initio* calculation for the interaction potential of the strongly interacting five-electron $\text{Li}^+ - \text{Li}$ system, which is for the first time precise enough to yield usable bounds for the ion-atom scattering length.

Rydberg molecules are key to the proposed method

in order to initialize the ultracold ion-atom scattering event. The binding in these molecules is established by the repeated elastic low-energy scattering between the quasifree Rydberg electron at position \mathbf{r} and the neutral but polarizable ground state atom at position \mathbf{R} relative to the ionic core. Fermi's pseudopotential [40], extended to include p -wave scattering [41], adequately describes this low-energy scattering:

$$\hat{V}_{eA}^T(\mathbf{r} - \mathbf{R}) = 2\pi a_0^T \delta^3(\mathbf{r} - \mathbf{R}) + 6\pi a_1^T \delta^3(\mathbf{r} - \mathbf{R}) \vec{\nabla} \cdot \vec{\nabla}, \quad (1)$$

where $a_l^T(k) = -\tan[\delta_l^T(k)]/k^{2l+1}$ is the energy-dependent triplet (T) s -wave ($l = 0$) and p -wave ($l = 1$) scattering length, respectively, as a function of the respective phase shifts $\delta_l^T(k)$ [42]. The wave number k of the Rydberg electron (the wave number of the ultracold ground state atom is negligible) at position \mathbf{R} is given by the semiclassical approximation $k(R)^2/2 = 1/R - 1/[2(\tilde{n}^*)^2]$, where \tilde{n}^* is the effective principal quantum number of the Rydberg level of interest [20]. The Rydberg molecule Hamiltonian, combining all three binary interactions between the Rydberg electron e , the Rydberg ionic core I , and the ground state atom A , then reads

$$\hat{H}_{AA}(\mathbf{r}, \mathbf{R}) = \hat{H}_{eI}(\mathbf{r}) + \hat{H}_{IA}^{\gg}(\mathbf{R}) + \hat{V}_{eA}^T(\mathbf{r} - \mathbf{R}) \hat{P}^T, \quad (2)$$

where \hat{H}_{eI} includes the spin-orbit coupling [42] and $\hat{H}_{IA}^{\gg}(\mathbf{R}) = \hat{\mathbf{P}}^2/(2\mu_{IA}) - C_4/(2R^4)$ describes the IA interaction at large internuclear distances, with $\hat{\mathbf{P}}$ and μ_{IA} being the momentum and the reduced mass, respectively. $\hat{P}^T = \hat{\mathbf{s}} \cdot \hat{\mathbf{s}} + 3/4$ is the triplet projection operator, with $\hat{\mathbf{s}}$ and $\hat{\mathbf{s}}$ the electronic spin of the Rydberg and the ground state electron, respectively. Applying the Born-Oppenheimer approximation then yields the nuclear Schrödinger equation $[\hat{\mathbf{P}}^2/(2\mu_{IA}) + V_{AA}(R)]\Psi_{AA}(\mathbf{R}) = E_{AA}\Psi_{AA}(\mathbf{R})$ with the spherically symmetric Rydberg molecule potentials V_{AA} , the Rydberg molecule wave functions Ψ_{AA} , and the corresponding binding energies E_{AA} calculated numerically [42]. The Rydberg molecule wave function of interest, $\tilde{\Psi}_{AA}$, is displayed in Fig. 2(a) for both lithium isotopes. It is bound in the $\text{Li}(30s_{1/2}) - \text{Li}(2s_{1/2})^3\Sigma$ Rydberg molecule potential \tilde{V}_{AA} , and it is in its rovibrational ground state ($\tilde{v} = \tilde{J} = 0$) [70], thus being spherically symmetric.

For the chosen Rydberg electron principal quantum number $\tilde{n} = 30$, the first excited vibrational state ($v = 1$) is approximately 5 MHz above the ground state, and the first excited rotational state ($J = 1$) is approximately $2\tilde{B} \approx 300$ kHz above the ground state [see Fig. 2(b)], where $B = (2\mu_{IA}r_{\text{cl}}^2)^{-1}$ is the rotational constant of the Rydberg molecule with the internuclear distance being approximated by the classical turning point $r_{\text{cl}} = 2(\tilde{n}^*)^2$ of the Rydberg electron. Hence, $2\tilde{B}$ is approximately 60 times larger than the typical Rydberg molecule decay linewidth γ_{AA} in a dilute atomic cloud [24, 25]. Besides, broadening mechanisms associated with the photoassociation of the Rydberg molecule (Doppler broadening, power broadening, laser linewidth, and finite laser

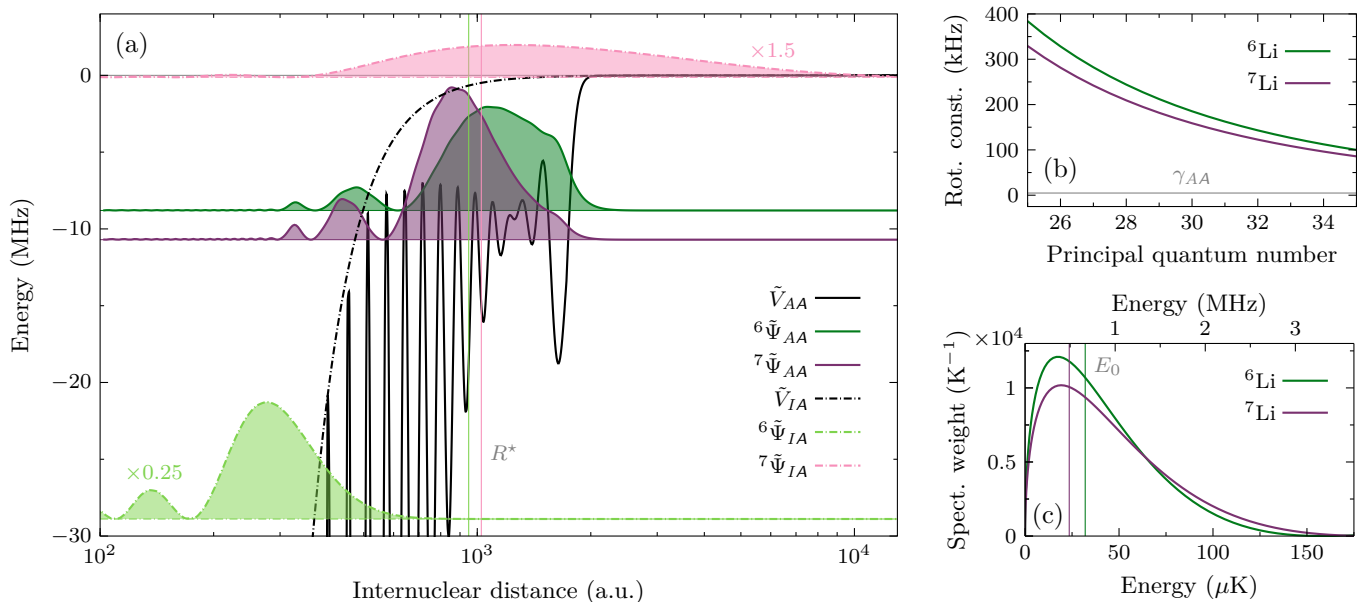


FIG. 2. Using Rydberg molecules to initialize an ultracold ion-atom scattering event, exemplified with lithium. The Rydberg molecule wave function of interest, more precisely, $R^2 |\tilde{\Psi}_{AA}(R)|^2$, is shown in (a) for both isotopes. It is bound in the homonuclear Li(30s)-Li(2s) potential $\tilde{V}_{AA}(R)$. It is in its spherically symmetric rovibrational ground state ($\tilde{\nu} = \tilde{J} = 0$), which can be experimentally addressed, evident from (b), as the rotational constant is larger than the Rydberg molecule decay linewidth γ_{AA} . Freed by photoionization, the initial Rydberg molecule wave function evolves in the spherically symmetric ion-atom interaction potential $\tilde{V}_{IA}(R)$, with R^* denoting its characteristic radius. Because of angular momentum conservation, only S -wave scattering occurs ($\tilde{J} = 0$) despite the components above E_0 in the Rydberg molecule energy spectrum; see (c). The overlap between $\tilde{\Psi}_{AA}$ and the last bound molecular ion wave function $\tilde{\Psi}_{IA}$ [see (a)] determines the bound fraction in the scattered wave packet.

pulse duration) can be made much smaller than $2\tilde{B}$ in an ultracold atomic cloud and with suitable laser parameters. Thus, the rovibrational ground state of the Rydberg molecule of interest can be experimentally addressed. Working with a spin-polarized atomic cloud and appropriate photoassociation laser polarization(s) also justifies neglecting singlet scattering between the Rydberg electron and the ground state atom [42]. Furthermore, focusing down the photoassociation laser(s) allows for the formation of a single Rydberg molecule per atomic cloud by means of the Rydberg blockade [71]. In combination with a dilute atomic cloud, this ensures that after photoionization there is only a single ion-atom scattering event happening at a time.

Photoionization frees the initial Rydberg molecule wave function by removing the Rydberg electron. Choosing a suitable photoionization scheme ensures, first, that the energy imparted onto the ion-atom system in the photoionization process is negligible in comparison with the S -wave scattering limit and, second, that the ionization process is fast compared to the effective trapping frequency of the Rydberg molecule potential [42]. This makes the photoionization diabatic; i.e., the shape of the initial Rydberg molecule wave function is preserved during ionization. The initial shape $\Psi_{IA}(\mathbf{R}, t = 0)$ of the

ion-atom wave packet is thus set for the subsequent ultracold scattering.

The scattering of the initial ion-atom wave packet is then described by the time-dependent Schrödinger equation

$$i\frac{\partial}{\partial t}\Psi_{IA}(\mathbf{R}, t) = \hat{H}_{IA}(\mathbf{R})\Psi_{IA}(\mathbf{R}, t), \quad (3)$$

where \hat{H}_{IA} is the nuclear Hamiltonian of the molecular ion [42], containing the spherically symmetric ground state molecular ion potential $\tilde{V}_{IA}(R)$. We carried out *ab initio* calculations to determine \tilde{V}_{IA} [42] which yielded a potential depth $D_e = 10468 \text{ cm}^{-1}$ with a conservatively estimated error of $\pm 10 \text{ cm}^{-1}$, thus in excellent agreement with the measured value of $(10464 \pm 6) \text{ cm}^{-1}$ [72]. For our molecular ion potential with $D_e = 10468 \text{ cm}^{-1}$, we calculate a ${}^6\text{Li}^+ - {}^6\text{Li}$ ion-atom doublet S -wave scattering length of $\mathcal{A}_6 = -1014 \text{ a.u.}$, with bounds $(\mathcal{A}_6^-, \mathcal{A}_6^+) = (-778; -1294) \text{ a.u.}$ corresponding to potentials scaled by (0.999; 1.001), respectively, reflecting our accuracy of 0.1% in D_e . For ${}^7\text{Li}^+ - {}^7\text{Li}$ we determine the scattering length \mathcal{A}_7 to be 7162 a.u. , with bounds of $(107825; 3664) \text{ a.u.}$ Hence, the scattering lengths differ considerably for the two lithium isotopes, with the magnitude of \mathcal{A}_6 being comparable to the characteristic radius of ion-atom interaction $R_6^* = \sqrt{\mu_{IA}C_4} =$

949 a.u. [11], whereas \mathcal{A}_7 is approximately 7 times $R_7^* = 1025$ a.u. This reflects also in the markedly dissimilar bounds we predict for the two scattering lengths, with tight bounds on \mathcal{A}_6 , while \mathcal{A}_7 is extremely sensitive to changes of the molecular ion potential. Correspondingly, the last bound molecular ion wave function ${}^7\tilde{\Psi}_{IA}$ has a large extension and accordingly a small binding energy, whereas ${}^6\tilde{\Psi}_{IA}$ is deeply bound at comparatively small internuclear distances, as can be seen in Fig. 2(a) (note the logarithmic scale for the internuclear distance). The vibrational molecular ion wave functions $\Psi_{IA}^v(\mathbf{R})$ and corresponding eigenenergies E_{IA}^v , with $\hat{H}_{IA}(\mathbf{R})\Psi_{IA}^v(\mathbf{R}) = E_{IA}^v\Psi_{IA}^v(\mathbf{R})$, are then used to express the scattered ion-atom wave packet in the form

$$\Psi_{IA}(\mathbf{R}, t) = \sum_v \pi_v e^{-iE_{IA}^v t} \Psi_{IA}^v(\mathbf{R}), \quad (4)$$

where the sum runs over bound ($E_{IA}^v < 0$) and scattering states ($E_{IA}^v > 0$) and $\pi_v = \langle \Psi_{IA}(\mathbf{R}, t=0) | \Psi_{IA}^v(\mathbf{R}) \rangle$ is the projection of the initial ion-atom wave packet on the vibrational state Ψ_{IA}^v . With the ion-atom interaction potential $\tilde{V}_{IA}(R)$ being spherically symmetric, and without an electric field \mathcal{E} present, the initial orbital angular momentum J of the ion-atom wave packet, given by the Rydberg molecule wave function, is conserved during scattering; i.e., scattering channels for different partial waves do not couple. Consequently, the molecular ion wave functions used to express the scattered wave packet in Eq. 4 have this very orbital angular momentum J . For the case studied in this Letter, where the initial Rydberg molecule wave function is in its spherically symmetric rotational ground state ($\tilde{J} = 0$), the orbital angular momentum conservation implies that only S -wave ion-atom scattering can occur despite the fact that $\tilde{\Psi}_{AA}$ has an energy spectrum with components above the S -wave scattering limit, as is illustrated in Fig. 2(c). The effect of electric stray fields $\mathcal{E}_{\text{stray}}$ is discussed in Supplemental Material [42].

We conducted ion-atom scattering calculations for both lithium isotopes, with $\Psi_{IA}(\mathbf{R}, t=0)$ given by the respective Rydberg molecule wave function $\tilde{\Psi}_{AA}$ displayed in Fig. 2(a), and for the respective ion-atom scattering length tuned over a wide range [42]. These calculations revealed two different scattering regimes depending on the scattering length \mathcal{A} . For positive scattering lengths, exemplarily illustrated in Fig. 3(a) for ${}^6\text{Li}^+ - {}^6\text{Li}$ scattering with a scattering length of $+R_6^*$, the scattered wave packet splits into a free, dispersively expanding shell and a bound shell, the position and shape of which reveal that the last bound molecular ion state has been formed. Both shells are spherically symmetric and thus demonstrate that only S -wave scattering occurs. For negative scattering lengths, the entire scattered wave packet is free as is exemplarily shown in Fig. 3(b) for ${}^6\text{Li}^+ - {}^6\text{Li}$ scattering with a scattering length of $-R_6^*$. This is due to the negligible overlap between the initial Rydberg

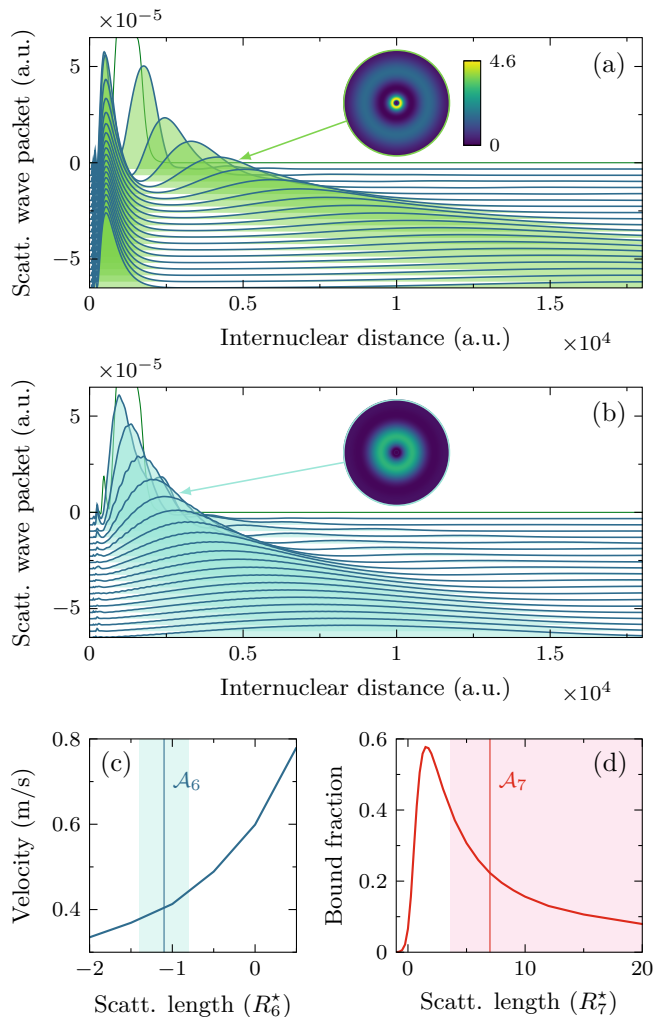


FIG. 3. Ultracold lithium ion-atom scattering processes, initialized with Rydberg molecules, for different scattering lengths \mathcal{A} . For $\mathcal{A} > 0$ [demonstrated in (a) for ${}^6\text{Li}^+ - {}^6\text{Li}$ scattering with $\mathcal{A} = +R_6^*$], the scattered wave packet splits into a free, expanding shell and a bound shell, indicating molecular ion formation. For $\mathcal{A} < 0$ [exemplified in (b) for $\mathcal{A} = -R_6^*$], the entire scattered wave packet is free. In (a) and (b), the time evolution of the scattered wave packet $R^2 |\Psi_{IA}(R, t)|^2$ is shown from $t = 0$ [$\Psi_{IA}(t=0) = \tilde{\Psi}_{AA}$, unfilled curve, vertical axis applies] to $1 \mu\text{s}$ in steps of 50 ns (top to bottom, curves shifted by -3.25×10^{-6} a.u. each). The insets demonstrate the S -wave character of the scattered wave packet [R extension of 7×10^3 a.u., same color scale in (a) and (b)]. For $\mathcal{A} > 0$ ($\mathcal{A} > 0$), the shell expansion velocity ζ (the bound fraction b) is a sensitive quantity to determine the scattering length; see (c) and (d), where also the scattering lengths $\mathcal{A}_{6,7}$ from our *ab initio* calculations are indicated (vertical lines with the shaded areas marking the bounds).

molecule wave function and the last bound molecular ion wave function, as can be seen in Fig. 2(a) for the example of ${}^6\tilde{\Psi}_{AA}$ and ${}^6\tilde{\Psi}_{IA}$ with $\mathcal{A}_6 = -1.1R_6^*$. In the regime of negative scattering lengths, the velocity ζ with which the maximum of the expanding shell moves is a sensitive

quantity to determine the scattering length, as can be seen from Fig. 3(c). With our predicted bounds on \mathcal{A}_6 , the ${}^6\text{Li}^+ - {}^6\text{Li}$ scattering falls into this regime. For positive scattering lengths, the bound fraction b of the total scattered ion-atom wave packet can be used to precisely determine the scattering length, as is demonstrated in Fig. 3(d) for ${}^7\text{Li}^+ - {}^7\text{Li}$ scattering, falling in this regime according to our scattering length calculations.

To experimentally measure the expansion velocity ζ , the freely moving scattered ion of a single ultracold scattering event is imaged onto a time- and position-sensitive single-ion detector. After many repetitions of this single scattering event, the scattered ion-atom wave packet can eventually be reconstructed, either in momentum space when, e.g., using a MOTRIMS [73] or VMI [74] apparatus or in real space when employing an ion microscope for imaging. Given the submicron resolution of these ion microscopes [75, 76], an evolution time in the microsecond range is sufficient to resolve the shape of the scattered wave packet. The bound fraction b can be measured in time of flight where the molecular ions Li_2^+ separate from the lighter free Li^+ ions. For guiding the ions onto the detector, a suitably small extraction electric field has to be used not to dissociate the weakly bound molecular ions.

The presented experimental method to use Rydberg molecules for the investigation of ultracold ion-atom scattering, particularized for the lithium ion-atom system in this Letter, is readily applicable to other ion-atom systems, e.g., to homo- or heteronuclear alkali or alkaline earth ion-atom systems for which Rydberg molecules can be formed [50, 77, 78]. In such a manner, the *ab initio* calculations of ion-atom scattering lengths could be benchmarked for increasingly complicated systems. Furthermore, having the ion-atom scattering lengths precisely determined with the proposed two-body scattering experiment would immediately allow for a more faithful and accurate description of the many-body, polaronic properties of an ion impurity immersed in an atomic quantum gas [79–83]. Finally, keeping the Rydberg electron as a spectator and Faraday cage for the ion-atom collision [84–88] might be possible also in the ultracold regime using circular Rydberg states [89].

We thank K. Jachymski and F. Merkt for fruitful discussions. We thank S. Hofferberth, K. Kleinbach, and F. Meinert for numerical code development to calculate Rydberg molecule potentials and wave functions. We acknowledge support from Deutsche Forschungsgemeinschaft [Projects No. PF 381/13-1 and No. PF 381/17-1, the latter being part of the SPP 1929 (GiRyd)], from the Czech Science Foundation (Project No. P208/14-15989P), and from the National Science Centre Poland (Project No. 2016/23/B/ST4/03231) as well as from the PL-Grid Infrastructure. C. V. acknowledges support from the Carl-Zeiss-Stiftung.

- [1] W. Ketterle, D. Durfee, and D. M. Stamper-Kurn, in *Bose-Einstein Condensation in Atomic Gases*, Proceedings of the International School of Physics “Enrico Fermi” Course CXL, edited by S. Stringari, M. Inguscio, and C. E. Wieman (IOS Press, Amsterdam, 1999) pp. 67–176.
- [2] W. Ketterle and M. W. Zwierlein, in *Ultracold Fermi Gases*, Proceedings of the International School of Physics “Enrico Fermi” Course CLXIV, edited by M. Inguscio, W. Ketterle, and C. Salomon (IOS Press, Amsterdam, 2008) pp. 95–287.
- [3] A. Härter and J. Hecker Denschlag, *Contemp. Phys.* **55**, 33 (2014).
- [4] D. Zhang and S. Willitsch, in *Cold Chemistry: Molecular Scattering and Reactivity Near Absolute Zero*, edited by O. Dulieu and A. Osterwalder (Royal Society of Chemistry, London, 2018) pp. 496–536.
- [5] M. Tomza, K. Jachymski, R. Gerritsma, A. Negretti, T. Calarco, Z. Idziaszek, and P. S. Julienne, arXiv:1708.07832v1 (2017).
- [6] Z. Meir, T. Sikorsky, R. Ben-shlomi, N. Akerman, Y. Dallah, and R. Ozeri, *Phys. Rev. Lett.* **117**, 243401 (2016).
- [7] A. Härter, A. Krüchow, A. Brunner, W. Schnitzler, S. Schmid, and J. Hecker Denschlag, *Phys. Rev. Lett.* **109**, 123201 (2012).
- [8] J. Joger, H. Fürst, N. Ewald, T. Feldker, M. Tomza, and R. Gerritsma, *Phys. Rev. A* **96**, 030703 (2017).
- [9] S. Schmid, A. Härter, and J. Hecker Denschlag, *Phys. Rev. Lett.* **105**, 133202 (2010).
- [10] R. Saito, S. Haze, M. Sasakawa, R. Nakai, M. Raoult, H. Da Silva, O. Dulieu, and T. Mukaiyama, *Phys. Rev. A* **95**, 032709 (2017).
- [11] C. Zipkes, S. Palzer, C. Sias, and M. Köhl, *Nature (London)* **464**, 388 (2010).
- [12] W. G. Rellergert, S. T. Sullivan, S. Kotochigova, A. Petrov, K. Chen, S. J. Schowalter, and E. R. Hudson, *Phys. Rev. Lett.* **107**, 243201 (2011).
- [13] S. T. Sullivan, W. G. Rellergert, S. Kotochigova, and E. R. Hudson, *Phys. Rev. Lett.* **109**, 223002 (2012).
- [14] F. H. J. Hall, P. Eberle, G. Hegi, M. Raoult, M. Aymar, O. Dulieu, and S. Willitsch, *Mol. Phys.* **111**, 2020 (2013).
- [15] F. H. J. Hall and S. Willitsch, *Phys. Rev. Lett.* **109**, 233202 (2012).
- [16] A. T. Grier, M. Cetina, F. Oručević, and V. Vuletić, *Phys. Rev. Lett.* **102**, 223201 (2009).
- [17] M. Cetina, A. T. Grier, and V. Vuletić, *Phys. Rev. Lett.* **109**, 253201 (2012).
- [18] T. Huber, A. Lambrecht, J. Schmidt, L. Karpa, and T. Schaetz, *Nat. Commun.* **5**, 5587 (2014).
- [19] A. Lambrecht, J. Schmidt, P. Weckesser, M. Debatin, L. Karpa, and T. Schaetz, *Nat. Photonics* **11**, 704 (2017).
- [20] C. H. Greene, A. S. Dickinson, and H. R. Sadeghpour, *Phys. Rev. Lett.* **85**, 2458 (2000).
- [21] V. Bendkowsky, B. Butscher, J. Nipper, J. P. Shaffer, R. Löw, and T. Pfau, *Nature (London)* **458**, 1005 (2009).
- [22] V. Bendkowsky, B. Butscher, J. Nipper, J. B. Balewski, J. P. Shaffer, R. Löw, T. Pfau, W. Li, J. Stanojevic, T. Pohl, and J. M. Rost, *Phys. Rev. Lett.* **105**, 163201 (2010).
- [23] A. Gaj, A. T. Krupp, J. B. Balewski, R. Löw, S. Hofferberth, and T. Pfau, *Nat. Commun.* **5**, 4546 (2014).

- [24] B. Butscher, V. Bendkowsky, J. Nipper, J. B. Balewski, L. Kukota, R. Löw, T. Pfau, W. Li, T. Pohl, and J. M. Rost, *J. Phys. B* **44**, 184004 (2011).
- [25] F. Camargo, J. D. Whalen, R. Ding, H. R. Sadeghpour, S. Yoshida, J. Burgdörfer, F. B. Dunning, and T. C. Killian, *Phys. Rev. A* **93**, 022702 (2016).
- [26] A. T. Krupp, A. Gaj, J. B. Balewski, P. Ilzhöfer, S. Hofferberth, R. Löw, T. Pfau, M. Kurz, and P. Schmelcher, *Phys. Rev. Lett.* **112**, 143008 (2014).
- [27] D. A. Anderson, S. A. Miller, and G. Raithel, *Phys. Rev. Lett.* **112**, 163201 (2014).
- [28] H. Saßmannshausen, F. Merkt, and J. Deiglmayr, *Phys. Rev. Lett.* **114**, 133201 (2015).
- [29] F. Böttcher, A. Gaj, K. M. Westphal, M. Schlagmüller, K. S. Kleinbach, R. Löw, T. C. Liebisch, T. Pfau, and S. Hofferberth, *Phys. Rev. A* **93**, 032512 (2016).
- [30] W. Li, T. Pohl, J. M. Rost, S. T. Rittenhouse, H. R. Sadeghpour, J. Nipper, B. Butscher, J. B. Balewski, V. Bendkowsky, R. Löw, and T. Pfau, *Science* **334**, 1110 (2011).
- [31] M. A. Bellos, R. Carollo, J. Banerjee, E. E. Eyler, P. L. Gould, and W. C. Stwalley, *Phys. Rev. Lett.* **111**, 053001 (2013).
- [32] D. Booth, S. T. Rittenhouse, J. Yang, H. R. Sadeghpour, and J. P. Shaffer, *Science* **348**, 99 (2015).
- [33] K. S. Kleinbach, F. Meinert, F. Engel, W. J. Kwon, R. Löw, T. Pfau, and G. Raithel, *Phys. Rev. Lett.* **118**, 223001 (2017).
- [34] T. Niederprüm, O. Thomas, T. Eichert, C. Lippe, J. Pérez-Ríos, C. H. Greene, and H. Ott, *Nat. Commun.* **7**, 12820 (2016).
- [35] M. Przybytek, W. Cencek, J. Komasa, G. Łach, B. Jeziorski, and K. Szalewicz, *Phys. Rev. Lett.* **104**, 183003 (2010).
- [36] M. Przybytek and B. Jeziorski, *J. Chem. Phys.* **123**, 134315 (2005).
- [37] S. Knoop, P. S. Żuchowski, D. Kędziera, Ł. Mentel, M. Puchalski, H. P. Mishra, A. S. Flores, and W. Vassen, *Phys. Rev. A* **90**, 022709 (2014).
- [38] D. Kędziera, Ł. Mentel, P. S. Żuchowski, and S. Knoop, *Phys. Rev. A* **91**, 062711 (2015).
- [39] A. Miffre, M. Jacquy, M. Büchner, G. Tréneç, and J. Vigué, *Eur. Phys. J. D* **38**, 353 (2006).
- [40] E. Fermi, *Nuovo Cimento* **11**, 157 (1934).
- [41] A. Omont, *J. Phys. (Paris)* **38**, 1343 (1977).
- [42] See Supplemental Material at <http://link.aps.org/supplemental/10.1103/PhysRevLett.120.153401>, which includes Refs. [18, 22, 43–69], for details on the Rydberg molecule calculations, the photoionization, the molecular ion calculations, and the ion-atom scattering simulations.
- [43] P. Goy, J. Liang, M. Gross, and S. Haroche, *Phys. Rev. A* **34**, 2889 (1986).
- [44] C.-J. Lorenzen and K. Niemax, *Phys. Scr.* **27**, 300 (1983).
- [45] B. A. Bushaw, W. Nörtershäuser, G. W. F. Drake, and H.-J. Kluge, *Phys. Rev. A* **75**, 052503 (2007).
- [46] M. Marinescu, H. R. Sadeghpour, and A. Dalgarno, *Phys. Rev. A* **49**, 982 (1994).
- [47] T. F. Gallagher, *Rydberg Atoms* (Cambridge University Press, Cambridge, England, 1994).
- [48] L. C. Biedenharn and J. D. Louck, *Angular Momentum in Quantum Physics: Theory and Application* (Cambridge University Press, Cambridge, England, 1984).
- [49] S. A. Bhatti, C. L. Cromer, and W. E. Cooke, *Phys. Rev. A* **24**, 161 (1981).
- [50] A.-L. Sinfailam and R. K. Nesbet, *Phys. Rev. A* **7**, 1987 (1973).
- [51] D. W. Norcross, *J. Phys. B* **4**, 1458 (1971).
- [52] H. R. Sadeghpour, J. L. Bohn, M. J. Cavagnero, B. D. Esry, I. I. Fabrikant, J. H. Macek, and A. R. P. Rau, *J. Phys. B* **33**, R93 (2000).
- [53] A. Beckmann, K. D. Böklen, and D. Elke, *Z. Phys.* **270**, 173 (1974).
- [54] C. Fey, M. Kurz, P. Schmelcher, S. T. Rittenhouse, and H. R. Sadeghpour, *New J. Phys.* **17**, 055010 (2015).
- [55] M. T. Eiles and C. H. Greene, *Phys. Rev. A* **95**, 042515 (2017).
- [56] L. J. Radziemski, R. Engleman, and J. W. Brault, *Phys. Rev. A* **52**, 4462 (1995).
- [57] P. M. Duarte, R. A. Hart, J. M. Hitchcock, T. A. Corcovilos, T.-L. Yang, A. Reed, and R. G. Hulet, *Phys. Rev. A* **84**, 061406 (2011).
- [58] M. Aymar, E. Luc-Koenig, and F. Combet Farnoux, *J. Phys. B* **9**, 1279 (1976).
- [59] P. J. Knowles, C. Hampel, and H.-J. Werner, *J. Chem. Phys.* **99**, 5219 (1993).
- [60] T. H. Dunning, Jr., *J. Chem. Phys.* **90**, 1007 (1989).
- [61] S. Boys and F. Bernardi, *Mol. Phys.* **19**, 553 (1970).
- [62] M. Reiher, *Theor. Chem. Acc.* **116**, 241 (2006).
- [63] H.-J. Werner *et al.*, MOLPRO, version 2015.1, a package of *ab initio* programs.
- [64] V. Kokouline, O. Dulieu, R. Kosloff, and F. Masnou-Seeuws, *J. Chem. Phys.* **110**, 9865 (1999).
- [65] M. Tomza, W. Skomorowski, M. Musiał, R. González-Férez, C. P. Koch, and R. Moszynski, *Mol. Phys.* **111**, 1781 (2013).
- [66] R. Kosloff, *Annu. Rev. Phys. Chem.* **45**, 145 (1994).
- [67] M. Tomza, M. H. Goerz, M. Musiał, R. Moszynski, and C. P. Koch, *Phys. Rev. A* **86**, 043424 (2012).
- [68] M. H. Goerz, D. M. Reich, M. Tomza, and C. P. Koch, QDYN, version 1.0, a program package for quantum dynamics and control.
- [69] A. Osterwalder and F. Merkt, *Phys. Rev. Lett.* **82**, 1831 (1999).
- [70] Here, the rovibrational ground state denotes the lowest-lying state with respect to the outermost well of the Rydberg molecule potential.
- [71] M. Saffman, T. G. Walker, and K. Mølmer, *Rev. Mod. Phys.* **82**, 2313 (2010).
- [72] R. A. Bernheim, L. P. Gold, T. Tipton, and D. D. Konowalow, *Chem. Phys. Lett.* **105**, 201 (1984).
- [73] S. Götz, B. Höltkemeier, C. S. Hofmann, D. Litsch, B. D. DePaola, and M. Weidemüller, *Rev. Sci. Instrum.* **83**, 073112 (2012).
- [74] B. J. Whitaker, ed., *Imaging in Molecular Dynamics: Technology and Applications* (Cambridge University Press, Cambridge, England, 2003).
- [75] A. Schwarzkopf, D. A. Anderson, N. Thaicharoen, and G. Raithel, *Phys. Rev. A* **88**, 061406 (2013).
- [76] M. Stecker, H. Schefzyk, J. Fortágh, and A. Günther, *New J. Phys.* **19**, 043020 (2017).
- [77] C. Bahrim, U. Thumm, and I. I. Fabrikant, *J. Phys. B* **34**, L195 (2001).
- [78] K. Bartschat and H. R. Sadeghpour, *J. Phys. B* **36**, L9 (2003).
- [79] R. Côté, V. Kharchenko, and M. D. Lukin, *Phys. Rev. Lett.* **89**, 093001 (2002).
- [80] P. Massignan, C. J. Pethick, and H. Smith, *Phys. Rev. A* **71**, 023606 (2005).

- [81] W. Casteels, J. Tempere, and J. T. Devreese, *J. Low Temp. Phys.* **162**, 266 (2011).
- [82] J. M. Schurer, P. Schmelcher, and A. Negretti, *Phys. Rev. A* **90**, 033601 (2014).
- [83] J. M. Schurer, A. Negretti, and P. Schmelcher, *New J. Phys.* **17**, 083024 (2015).
- [84] S. T. Pratt, J. L. Dehmer, P. M. Dehmer, and W. A. Chupka, *J. Chem. Phys.* **101**, 882 (1994).
- [85] B. R. Strazisar, C. Lin, and H. F. Davis, *Phys. Rev. Lett.* **86**, 3997 (2001).
- [86] E. Wrede, L. Schnieder, K. Seekamp-Schnieder, B. Niederjohann, and K. H. Welge, *Phys. Chem. Chem. Phys.* **7**, 1577 (2005).
- [87] D. Dai, C. C. Wang, G. Wu, S. A. Harich, H. Song, M. Hayes, R. T. Skodje, X. Wang, D. Gerlich, and X. Yang, *Phys. Rev. Lett.* **95**, 013201 (2005).
- [88] P. Allmendinger, J. Deiglmayr, K. Höveler, O. Schullian, and F. Merkt, *J. Chem. Phys.* **145**, 244316 (2016).
- [89] M. Matsuzawa, *Phys. Rev. A* **82**, 054701 (2010).

SUPPLEMENTAL MATERIAL for: “Rydberg Molecules for Ion-Atom Scattering in the Ultracold Regime”

Rydberg molecule calculations

In the following, the calculation of Rydberg molecule wave functions and binding energies is thoroughly discussed. First, two of the three binary interactions of the three-body Rydberg molecule Hamiltonian (see Eq. 2 and Fig. S1) are detailed, namely the Rydberg-electron – Rydberg-ionic-core interaction and the Rydberg-electron – ground-state-atom interaction. Afterwards, the solution of the complete Rydberg molecule Hamiltonian by applying the Born-Oppenheimer approximation, i.e., by treating the electronic and nuclear degrees of freedom sequentially, is particularized.

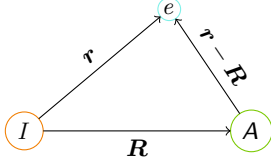


FIG. S1. Schematic illustration of the Rydberg molecule AA , constituting a three-body system where the Rydberg electron e binds the neutral, polarizable ground state atom A to the Rydberg ionic core I .

Rydberg-electron – Rydberg-ionic-core interaction

The Schrödinger equation for the Rydberg-electron – Rydberg-ionic-core interaction reads

$$\left[\frac{\hat{\mathbf{p}}^2}{2\mu_{eI}} + \hat{V}_{eI}(r) \right] \psi_{nljm_j}(\mathbf{r}) = E_{nlj} \psi_{nljm_j}(\mathbf{r}), \quad (\text{S1})$$

where $\hat{\mathbf{p}}$ is the Rydberg electron momentum, μ_{eI} is the reduced electron – ionic-core mass, which is approximated with the bare electron mass m_e in the following, $\hat{V}_{eI}(r)$ is the spherically symmetric interaction potential, ψ_{nljm_j} are the Rydberg electron wave functions, and E_{nlj} are the corresponding eigenenergies.

For $l \leq 2$, the eigenenergies E_{nlj} are calculated via

$$E_{nlj} = -\frac{\mathcal{R}^*}{(n^*)^2}, \quad (\text{S2})$$

where n^* is the effective principal quantum number given by

$$n^* = n - \delta_{nlj}, \quad (\text{S3})$$

with the quantum defect

$$\delta_{nlj} = \delta_0 + \frac{\delta_2}{(n - \delta_0)^2} + \frac{\delta_4}{(n - \delta_0)^4} + \frac{\delta_6}{(n - \delta_0)^6} + \dots \quad (\text{S4})$$

(see Table SI for the used values for lithium), and where \mathcal{R}^* is the reduced Rydberg constant (given in Table SII for lithium). For $l \geq 3$, the eigenenergies are calculated with [S5]

$$E_{nlj} = -\mathcal{R}^* \left[\frac{1}{n^2} + \frac{\alpha_{\text{fs}}^2}{n^3} \left(\frac{1}{j+1/2} - \frac{3}{4n} \right) \right] - \frac{3\alpha_c}{4n^3 l^5}, \quad (\text{S5})$$

where α_{fs} is the fine structure constant, and α_c is the ionic core polarizability (see Table SII for the lithium value).

For $\hat{V}_{eI}(r)$, the following model potential is used [S4]:

$$\hat{V}_{eI}(r) = V_C(r) + V_p(r) + \hat{V}_{\text{so}}(r), \quad (\text{S6})$$

with the Coulomb term

$$V_C(r) = -\frac{Z_l(r)}{r}, \quad (\text{S7})$$

Z_l being the radial charge distribution

$$Z_l(r) = 1 + (Z - 1)e^{-\alpha_1 r} - r(\alpha_3 + \alpha_4 r)e^{-\alpha_2 r}, \quad (\text{S8})$$

with the nuclear charge Z and $\alpha_{1,2,3,4}$ model parameters (see Ref. [S4] for lithium values); V_p is the core polarization term

$$V_p(r) = -\frac{\alpha_c}{2r^4} \left[1 - e^{-(r/r_c)^6} \right], \quad (\text{S9})$$

with r_c the effective core size (see Ref. [S4]); \hat{V}_{so} is the spin-orbit coupling term for which the approximation

$$\hat{V}_{\text{so}}(r > r_c) = \frac{\alpha_{\text{fs}}^2}{2r^3} \hat{\mathbf{l}} \cdot \hat{\mathbf{s}} \quad (\text{S10})$$

is used, valid in the region $r > r_c$. For calculating Rydberg wave functions, this approximation is justified.

To solve the Schrödinger equation S1 for the Rydberg electron wave functions, the separation ansatz

$$\psi_{nljm_j}(\mathbf{r}) = R_{nlj}(r) \mathcal{Y}_{(l)jm_j}(\vartheta, \varphi) \quad (\text{S11})$$

is made, where $\mathcal{Y}_{(l)jm_j}$ are the spin spherical harmonics for $s = 1/2$, thus $l = j \pm 1/2$, given in matrix form by [S6]

$$\mathcal{Y}_{(j \pm \frac{1}{2})jm_j} = \frac{1}{\sqrt{2(j \pm \frac{1}{2}) + 1}} \times \begin{pmatrix} \mp \sqrt{j \pm \frac{1}{2} \mp m_j + \frac{1}{2}} Y_{j \pm \frac{1}{2}}^{m_j - \frac{1}{2}} \\ \sqrt{j \pm \frac{1}{2} \pm m_j + \frac{1}{2}} Y_{j \pm \frac{1}{2}}^{m_j + \frac{1}{2}} \end{pmatrix}, \quad (\text{S12})$$

with Y_l^m being the spherical harmonics. The spin-orbit term acting on this ansatz yields

$$\begin{aligned} \hat{V}_{\text{so}} \psi_{nljm_j} &= \frac{\alpha_{\text{fs}}^2}{4r^3} \left[j(j+1) - l(l+1) - \frac{3}{4} \right] \psi_{nljm_j} \\ &= \mathcal{Y}_{(l)jm_j} V_{\text{so}} R_{nlj}, \end{aligned} \quad (\text{S13})$$

TABLE SI. Lithium quantum defects used in this Letter.

Isotope	State	δ_0	δ_2	δ_4	δ_6	Ref.
6, 7	$s_{1/2}$	0.399 510 1	0.0290			[S1]
6	$p_{1/2}$	0.047 183 5	-0.024			[S1]
6	$p_{3/2}$	0.047 172 0	-0.024			[S1]
7	$p_{1/2}$	0.047 178 0	-0.024			[S1]
7	$p_{3/2}$	0.047 166 5	-0.024			[S1]
6, 7	$d_{3/2}, d_{5/2}$	0.002 129	-0.014 91	0.1759	-0.8507	[S2]

TABLE SII. Lithium reduced Rydberg constants \mathcal{R}^* and lithium ionic core polarizability α_c used in this Letter.

Quantity	Isotope	Value	Ref.
\mathcal{R}^* (THz)	6	3289.541 926	[S1]
\mathcal{R}^* (THz)	7	3289.584 728 32	[S3]
α_c (a.u.)	6, 7	0.1923	[S4]

where

$$V_{\text{so}}(r) = \frac{\alpha_{\text{fs}}^2}{4r^3} [j(j+1) - l(l+1) - s(s+1)] \quad (\text{S14})$$

was introduced with $s = 1/2$. The radial part R_{nlj} of the electron wave functions is then found solving

$$\left[-\frac{1}{2r} \frac{d^2}{dr^2} r + \frac{l(l+1)}{2r^2} + V_{eI}(r) \right] R_{nlj}(r) = E_{nlj} R_{nlj}(r) \quad (\text{S15})$$

with a square root rescaling of r [S7] and by using Numerov's method for numerical integration.

Rydberg-electron – ground-state-atom interaction

As outlined in the main article, the Rydberg-electron – ground-state-atom interaction potential is given by Eq. 1, where the energy-dependent triplet s - and p -wave phase shifts $\delta_l^T(k)$ are used to calculate the respective scattering lengths $a_l^T(k)$. For the lithium system used in this Letter to exemplify the proposed method for ultracold ion-atom scattering, we conducted R -matrix calculations to determine the electron-lithium scattering phase shifts. These phase shifts are displayed in Fig. S2, and characteristic quantities extracted from them are given in Table SIII. Our phase shifts feature a better accuracy than previously published values (see Table SIII), especially at very low scattering energies, which is necessary to faithfully represent the low-energy scattering between the Rydberg electron and the ground state atom.

For internuclear distances larger than the classical turning point of the Rydberg electron, the semiclassical approximation

$$\frac{k^2}{2} = \frac{1}{R} - \frac{1}{2(n^*)^2} \quad (\text{S16})$$

for the scattering energy $E = k^2/2$ ceases to be applicable. Additionally, for the polarization potential, the p -wave scattering lengths diverge in the zero-energy limit [S10]. Therefore, a cutoff energy is defined below which, in Eq. 1, the zero-energy s -wave scattering lengths are used and the p -wave scattering lengths are set to zero. This cutoff energy is defined such that the Rydberg molecule potential of interest \tilde{V}_{AA} is smooth at the classical turning point. It is approximately 0.276 meV for the \tilde{V}_{AA} shown in Fig. 2(a).

In this Letter, singlet scattering between the Rydberg electron and the ground state atom is neglected as well as the hyperfine interaction in the ground state atom. This yields a prototypical Rydberg molecule as for example in Ref. [S11] which is, for its simplicity, well suited to demonstrate the proposed method for ultracold ion-atom scattering. Conducting the experiment with stretched states of the Rydberg and the ground state electron (e.g., $m_s = m_s = +1/2$), and that the depth of the Rydberg molecule potential of interest in the range given by the extension of $\tilde{\Psi}_{AA}$ is much smaller than the hyperfine splitting in the lithium ground state atom {approximately 228 MHz for ${}^6\text{Li}$ and 804 MHz for ${}^7\text{Li}$ [S12] in comparison with about 30 MHz; see Fig. 2(a)} guarantees that these two omissions are justified.

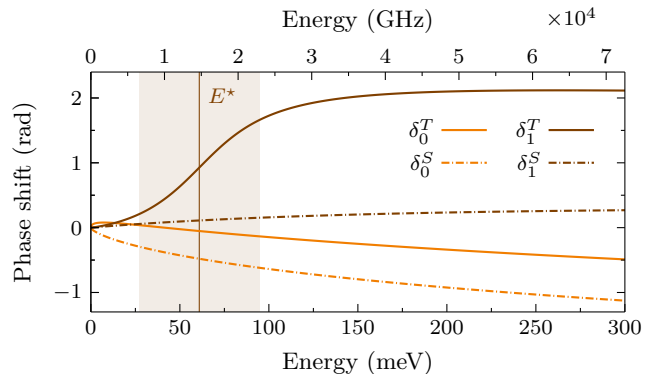


FIG. S2. Non-isotope-specific electron-lithium scattering phase shifts $\delta_l^{S,T}$ as a function of energy E for singlet (S) and triplet (T), s -wave ($l = 0$) and p -wave ($l = 1$) scattering. The triplet p -wave shape resonance position E^* and width Γ^* (shaded area) are also indicated (the values are given in Table SIII). The presented phase shifts feature a high accuracy at low scattering energies.

TABLE III. Electron-lithium scattering: characteristic quantities and accuracy considerations. Given are the zero-energy singlet (S) and triplet (T) s -wave ($l = 0$) scattering lengths $\bar{a}_0^{S,T}$ and the triplet p -wave shape resonance position E^* and width Γ^* . Our values (PW: present work) are in good agreement with previously published ones, except for Γ^* where the deviation might be attributed to convergence issues in the calculations of Ref. [S8]. Comparing the minimum scattering energies E_{\min} down to which the respective phase shift calculations were conducted and the results tabulated (with the energy resolution being on the same order as E_{\min}) indicates the improved accuracy of our calculations, especially at low scattering energies. This, in turn, renders our zero-energy scattering lengths particularly sound.

\bar{a}_0^T (a.u.)	\bar{a}_0^S (a.u.)	E^* (meV)	Γ^* (meV)	E_{\min} (meV)	Ref.
-7.43	2.99	60.9	67.9	0.023	PW
-7.12	3.04			0.136	[S9]
		60	57	34	[S8]

Solving the electronic Schrödinger equation

Treating the nuclear coordinates as parameters, the electronic Schrödinger equation of the Rydberg molecule reads

$$\hat{H}_{AA}(\mathbf{r}; R)\psi_{AA}(\mathbf{r}; R) = V_{AA}(R)\psi_{AA}(\mathbf{r}; R), \quad (\text{S17})$$

where

$$\hat{H}_{AA}(\mathbf{r}; R) = \hat{H}_{eI}(\mathbf{r}) + V_{IA}^{\gg}(R) + \hat{V}_{eA}^T(\mathbf{r} - R\mathbf{e}_z)\hat{P}^T \quad (\text{S18})$$

is the electronic Hamiltonian with $\hat{H}_{eI}(\mathbf{r})$ given in Eq. S1, with $V_{IA}^{\gg}(R) = -C_4/(2R^4)$ as the ion-atom interaction potential valid at large internuclear distances, and with $\hat{V}_{eA}^T(\mathbf{r} - R\mathbf{e}_z)$ given by Eq. 1, where \mathbf{R} was chosen to lie along the z axis, $\mathbf{R} = R\mathbf{e}_z$, without loss of generality. To solve for the electronic Rydberg molecule orbitals (MO) $\psi_{AA}(\mathbf{r}; R)$ and the corresponding spherically symmetric Rydberg molecule potentials $V_{AA}(R)$, the Schrödinger equation S17 is numerically diagonalized for each R in the basis $\{|n, l, j, m_j; \mathbf{m}_s\rangle\}$ of Rydberg electron wave functions $\psi_{nljm_j}(\mathbf{r})$ (see Eq. S11) multiplied with the spin state $|\mathbf{m}_s\rangle$ of the ground state atom's valence electron ($\mathbf{m}_s = \pm 1/2$ for lithium). The infinite number of basis states of different n is reduced to comprise four total manifolds, two below and one above the manifold containing the Rydberg level of interest; i.e., for lithium with zero integer parts of the quantum defects (see Table SI) $n = \tilde{n} - 2, \tilde{n} - 1, \tilde{n}, \tilde{n} + 1$, with \tilde{n} indicating the principal quantum number of the Rydberg level of interest. This was shown to yield accurate Rydberg molecule potentials [S13, S14]. The orbital angular quantum number l is not truncated, thus $l = 0, \dots, n-1$. With merely s - and p -wave scattering included (see Eq. 1), only basis states with $|m_j| \leq 3/2$ contribute since the spherical harmonics vanish on the z axis except for $m_l = 0$. Obtaining the

same number of electronic Rydberg MO's ψ_{AA} and corresponding potentials V_{AA} as the number of basis states included in the diagonalization, a counting index N is introduced for unambiguous identification, with $\tilde{N} = 0$ for the MO and potential of interest, i.e., $\tilde{\psi}_{AA} = \psi_0$ and $\tilde{V}_{AA} = V_0$. Alternatively, the MO and potential of interest are labeled with the term symbol $30s_{1/2}\sigma\ 2s_{1/2}\sigma\ ^3\Sigma_0$.

Solving the nuclear Schrödinger equation

The Rydberg molecule potentials obtained by solving the electronic Schrödinger equation S17 enter the nuclear Schrödinger equation of the Rydberg molecule in the form

$$\left[\frac{\hat{P}^2}{2\mu_{IA}} + V_N(R) \right] \Psi_{NvJ}(\mathbf{R}) = E_{NvJ} \Psi_{NvJ}(\mathbf{R}), \quad (\text{S19})$$

where $\Psi_{NvJ}(\mathbf{R})$ is the nuclear Rydberg MO, also denoted Rydberg molecule wave function, bound in the N 'th Rydberg molecule potential, with v and J indicating the vibrational and rotational state, respectively; E_{NvJ} is the corresponding Rydberg molecule binding energy. Making the separation ansatz

$$\Psi_{NvJ}(\mathbf{R}) = R_{NvJ}(R)\mathcal{P}_J(\theta) \quad (\text{S20})$$

with the normalized Legendre polynomials

$$\mathcal{P}_J(\theta) = \sqrt{\frac{2J+1}{4\pi}} P_J(\theta) \quad (\text{S21})$$

for the angular part then yields the one-dimensional radial Schrödinger equation

$$\left[-\frac{1}{2\mu_{IA}} \frac{1}{R} \frac{d^2}{dR^2} R + \frac{J(J+1)}{2\mu_{IA}R^2} + V_N(R) \right] R_{NvJ}(R) = E_{NvJ} R_{NvJ}(R), \quad (\text{S22})$$

which is solved for the radial part $R_{NvJ}(R)$ and binding energy E_{NvJ} by applying a square root rescaling of R [S7] and subsequent numerical integration using Numerov's method.

Photoionization

We propose a V -type photoionization scheme to free the initial Rydberg molecule wave function in order to start the ultracold ion-atom scattering. Applying this scheme as displayed in Fig. S3 to the lithium Rydberg molecule wave function of interest $\tilde{\Psi}_{AA}$, with the two ionization laser beams copropagating and with the ascending laser tuned maximally 1 GHz above the ionization threshold, the energy imparted onto the ion-atom system is more than 10 times smaller than the respective

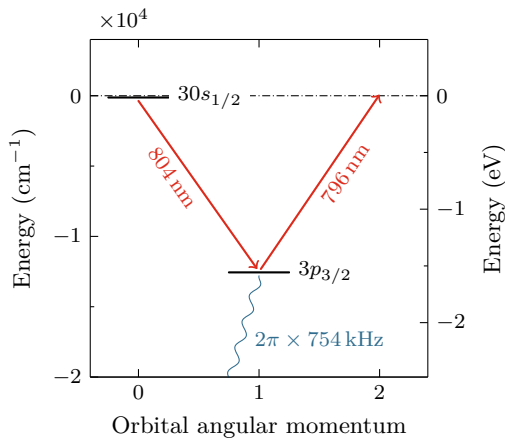


FIG. S3. V-type photoionization scheme to remove the Rydberg electron of the initial Rydberg molecule in order to start the ultracold ion-atom scattering. Here, this scheme is illustrated for lithium, with the Rydberg electron initially in the $30s_{1/2}$ state and subsequently brought into the continuum with two lasers via the $3p_{3/2}$ state (the dash-dotted line indicates the ionization threshold). The energy $E_{30s_{1/2}}$ is calculated with Eq. S2, $E_{3p_{3/2}}$ is determined from references [S3, S15], and the total decay rate of the $3p_{3/2}$ state (both into the $3s_{1/2}$ and the $2s_{1/2}$ state) is taken from Ref. [S16].

S-wave scattering limit of the two lithium isotopes. The photoionization process is diabatic as long as its timescale is considerably faster than the trapping frequencies of the Rydberg molecule potential in which $\tilde{\Psi}_{AA}$ is bound. For the photoionization process depicted in Fig. S3, with an ionization cross section taken from Ref. [S17] and for typical ionization laser parameters (i.e., for typical laser powers and beam waists), we calculate a photoionization timescale of a few nanoseconds, corresponding to a frequency of a few tens of megahertz. It is thus significantly larger than the effective radial trapping frequency one can attribute to the Rydberg molecule potential of interest \tilde{V}_{AA} by averaging the zero-point energy over the main extension range of $\tilde{\Psi}_{AA}$ [see Fig. 2(a)]. In contrast to the radial direction, there is no angular confinement present for $\tilde{\Psi}_{AA}$. Consequently, the photoionization process of the lithium initial Rydberg molecule wave function is diabatic.

Molecular ion calculations

In the following, our *ab initio* calculations of the lithium ground state molecular ion potential \tilde{V}_{IA} , also denoted as ion-atom interaction potential, are detailed. We treat the lithium molecular ion as a seven-body system where the altogether five electrons bind the two triply-charged bare ionic cores together (see Fig. S4). As opposed to the three-body Rydberg molecule system (see Fig. S1), where the Rydberg electron is singled out and

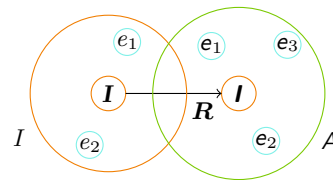


FIG. S4. Schematic illustration of the lithium molecular ion IA studied in this Letter, constituting a seven-body system where in total five electrons (two electrons e_i from the Rydberg ionic core I and three electrons e_j from the ground state atom A) bind the two triply-charged bare ionic cores I and I together.

the remaining electrons enter the Rydberg molecule calculations only implicitly, for our molecular ion calculations, all electrons are treated on equal footing.

We apply the Born-Oppenheimer approximation to our five-electron – two-nuclei lithium molecular ion system in order to separate the electronic from the nuclear degrees of freedom. This yields the electronic Schrödinger equation, the solution of which in turn yields the spherically symmetric molecular ion potentials $V_{IA}(R)$. For our ion-atom scattering calculations, only the ground state molecular ion potential $\tilde{V}_{IA}(R)$ is of interest (see Eq. S23). To solve the electronic Schrödinger equation for \tilde{V}_{IA} , we use coupled cluster methods with Gaussian basis sets. In the first step, we use the spin-restricted open-shell coupled cluster method restricted to single, double, and non-iterative triple excitations, starting from the restricted open-shell Hartree-Fock orbitals, RCCSD(T) [S18], and the augmented correlation-consistent polarized core-valence quintuple- ζ quality basis set (aug-cc-pCV5Z) [S19]. The interaction energy is obtained with the supermolecule method and the basis set superposition error is corrected by using the counterpoise correction [S20]. Next, the remaining contribution of the full triple excitations in the coupled cluster method (RCCSDT) is calculated with a smaller basis set (aug-cc-pCVTZ) and added to the full interaction potential. The importance of the scalar relativistic effects is assessed by performing coupled cluster calculations with the third-order Douglas-Kroll-Hess Hamiltonian [S21]. The uncertainty of the obtained molecular ion potential is evaluated by a systematic convergence analysis of the results obtained with different basis sets and methods. The electronic structure calculations are performed with the MOLPRO package of *ab initio* programs [S22].

The resulting $\text{Li}^+ - \text{Li}(2s_{1/2}) X^2\Sigma$ ground state molecular ion potential \tilde{V}_{IA} is displayed in Fig. 2(a). For internuclear distances R being much larger than the equilibrium distance R_e of the molecular ion potential, \tilde{V}_{IA} transitions into the polarization potential $\tilde{V}_{IA}^{\gg} = -C_4/(2R^4)$.

Ion-atom scattering calculations

The scattering of the initial ion-atom wave packet $\Psi_{IA}(\mathbf{R}, t = 0)$ is described by the time-dependent Schrödinger equation 3 in which the nuclear Hamiltonian of the molecular ion is given by

$$\hat{H}_{IA}(\mathbf{R}) = \frac{\hat{\mathbf{P}}^2}{2\mu_{IA}} + \tilde{V}_{IA}(R), \quad (\text{S23})$$

where $\hat{\mathbf{P}}$ is the momentum and μ_{IA} the reduced mass of the molecular ion system IA (see Fig. S4), and $\tilde{V}_{IA}(R)$ is the ground state molecular ion potential.

For the spatial and temporal propagation of the initial ion-atom wave packet, the radial part of the scattering Hamiltonian \hat{H}_{IA} is represented on a Fourier grid with an adaptive step size [S23] and the angular part is expanded in terms of Legendre polynomials [S24]. Without an electric field, the scattering Hamiltonian is diagonalized and its eigenstates and eigenenergies are used in propagation as given by Eq. 4. In an electric field, we propagate the wave packet using the Chebyshev propagator [S25, S26]. To enable propagation times over microseconds and internuclear distances over 10^5 a.u., we use a reduced ion-atom interaction potential which supports only several bound vibrational states and has the same long-range part and scattering length as the original potential. We have found that reduced potentials supporting four or more vibrational states give the same scattering results. The reduced interaction potential is obtained by adding a repulsive C_{12}/R^{12} barrier to the original potential. By adjusting C_{12} , we set the number of vibrational states and we control the scattering length. We employ up to 11 partial waves and as many as 8192 radial grid points with a maximum internuclear distance of up to 5×10^5 a.u. The scattering calculations are performed with the developer version of the QDYN program package [S27].

Without an electric field present, only S -wave scattering occurs and hence the scattered ion-atom wave packet is spherically symmetric [see inset in Fig. 3(a) and 3(b), respectively]. Electric stray fields $\mathcal{E}_{\text{stray}}$ during the scattering process admix higher partial waves to the scattered wave packet and thus break its spherical symmetry. We performed scattering calculations showing that for any $\mathcal{E}_{\text{stray}} \leq 0.1$ mV/cm the introduced asymmetry in the scattered wave packet is small enough to still yield the same expansion velocity ζ and bound fraction b , and hence the same scattering length \mathcal{A} , as in the electric-field-free case [see Fig. 3(c) and 3(d), respectively]. An $\mathcal{E}_{\text{stray}} \leq 0.1$ mV/cm is experimentally achievable with suitable compensation schemes [S28, S29].

- [S1] P. Goy, J. Liang, M. Gross, and S. Haroche, Phys. Rev. A **34**, 2889 (1986).
- [S2] C.-J. Lorenzen and K. Niemax, Phys. Scr. **27**, 300 (1983).
- [S3] B. A. Bushaw, W. Nörtershäuser, G. W. F. Drake, and H.-J. Kluge, Phys. Rev. A **75**, 052503 (2007).
- [S4] M. Marinescu, H. R. Sadeghpour, and A. Dalgarno, Phys. Rev. A **49**, 982 (1994).
- [S5] T. F. Gallagher, *Rydberg Atoms* (Cambridge University Press, Cambridge, England, 1994).
- [S6] L. C. Biedenharn and J. D. Louck, *Angular Momentum in Quantum Physics: Theory and Application* (Cambridge University Press, Cambridge, England, 1984).
- [S7] S. A. Bhatti, C. L. Cromer, and W. E. Cooke, Phys. Rev. A **24**, 161 (1981).
- [S8] A.-L. Sinfailam and R. K. Nesbet, Phys. Rev. A **7**, 1987 (1973).
- [S9] D. W. Norcross, J. Phys. B **4**, 1458 (1971).
- [S10] H. R. Sadeghpour, J. L. Bohn, M. J. Cavagnero, B. D. Esry, I. I. Fabrikant, J. H. Macek, and A. R. P. Rau, J. Phys. B **33**, R93 (2000).
- [S11] V. Bendkowsky, B. Butscher, J. Nipper, J. B. Balewski, J. P. Shaffer, R. Löw, T. Pfau, W. Li, J. Stanojevic, T. Pohl, and J. M. Rost, Phys. Rev. Lett. **105**, 163201 (2010).
- [S12] A. Beckmann, K. D. Böklen, and D. Elke, Z. Phys. **270**, 173 (1974).
- [S13] C. Fey, M. Kurz, P. Schmelcher, S. T. Rittenhouse, and H. R. Sadeghpour, New J. Phys. **17**, 055010 (2015).
- [S14] M. T. Eiles and C. H. Greene, Phys. Rev. A **95**, 042515 (2017).
- [S15] L. J. Radziemski, R. Engleman, and J. W. Brault, Phys. Rev. A **52**, 4462 (1995).
- [S16] P. M. Duarte, R. A. Hart, J. M. Hitchcock, T. A. Corcovilos, T.-L. Yang, A. Reed, and R. G. Hulet, Phys. Rev. A **84**, 061406 (2011).
- [S17] M. Aymar, E. Luc-Koenig, and F. Combet Farnoux, J. Phys. B **9**, 1279 (1976).
- [S18] P. J. Knowles, C. Hampel, and H.-J. Werner, J. Chem. Phys. **99**, 5219 (1993).
- [S19] T. H. Dunning, Jr., J. Chem. Phys. **90**, 1007 (1989).
- [S20] S. Boys and F. Bernardi, Mol. Phys. **19**, 553 (1970).
- [S21] M. Reiher, Theor. Chem. Acc. **116**, 241 (2006).
- [S22] H.-J. Werner *et al.*, MOLPRO, version 2015.1, a package of *ab initio* programs.
- [S23] V. Kokouline, O. Dulieu, R. Kosloff, and F. Masnou-Seeuws, J. Chem. Phys. **110**, 9865 (1999).
- [S24] M. Tomza, W. Skomorowski, M. Musiał, R. González-Férez, C. P. Koch, and R. Moszynski, Mol. Phys. **111**, 1781 (2013).
- [S25] R. Kosloff, Annu. Rev. Phys. Chem. **45**, 145 (1994).
- [S26] M. Tomza, M. H. Goerz, M. Musiał, R. Moszynski, and C. P. Koch, Phys. Rev. A **86**, 043424 (2012).
- [S27] M. H. Goerz, D. M. Reich, M. Tomza, and C. P. Koch, QDYN, version 1.0, a program package for quantum dynamics and control.
- [S28] A. Osterwalder and F. Merkt, Phys. Rev. Lett. **82**, 1831 (1999).
- [S29] T. Huber, A. Lambrecht, J. Schmidt, L. Karpa, and T. Schaetz, Nat. Commun. **5**, 5587 (2014).